Submitted to Physical Review A

LBL-2440
Preprint

MULTI-IONIZATION OF NEON, ARGON AND XENON AND THEIR IONS BY HIGH ENERGY ELECTRON IMPACT

Arthur Salop

December 18, 1973

Prepared for the U.S. Atomic Energy Commission under Contract W-7405-ENG-48

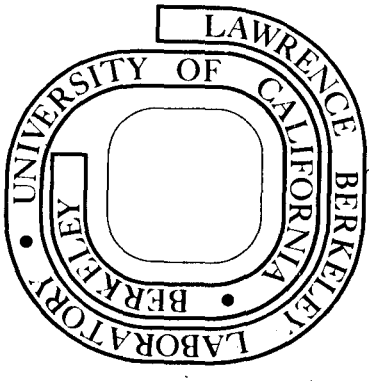

DISCLAIMER

Multi-Ionization of Neon, Argon and Xenon and their Ions by High Energy Electron Impact*

Arthur Salop

Lawrence Berkeley Laboratory
University of California
Berkeley, California

December 18, 1973

* Work done under the auspices of the U.S. Atomic Energy Commission.

Abstract

Estimates have been made of the total ionization cross sections for the collision of high energy electrons with neon, argon and xenon atoms and all of their ground state ions. The cross sections were computed within the framework of the Bethe-Born high-energy-approximation theory using the semi-classical projection-operator technique of Hahn and Watson and the independent-particle model for atoms of Green, Sellin and Zachor. Both direct continuum ionization and inner shell excitation followed by Auger transitions were taken into account. Multiple-ionization cross sections were also estimated using experimental data on electron emission following ejection of inner-shell electrons in the various rare gas atoms and a simplified model of Auger vacancy cascading in ions. The computed cross section values were then used in calculations of the cumulative ionization produced by a relativistic electron ring beam interacting initially with pressure pulses of the various gases. The results obtained, taken together with previous computations for krypton, indicate a progressive increase in the relative importance of Auger processes with increase in Z such that for xenon (and presumably for higher-Z target atoms), Auger ionization dominates the production rates of most of the multi-charged ions formed in such a system.

I. Introduction

In a previous paper,[1] estimates were obtained of total ionization and multi-ionization high energy-electron collision cross sections for krypton and its ground state ions. The computations were motivated by the need for such information in the design, development and analysis of electron ring

devices[2,3] and other heavy ion sources utilizing ion trapping and ionization by successive electron impact.[4,5]

The total cross sections (for ejection of one or more electrons) were computed within the framework of the Bethe-Born[6,7] high energy approximation theory using the semi-classical projection-operator technique of Hahn and Watson[8,9] and the independent particle model (IPM) atomic potential due to Green, Sellin, and Zachor.[10] Both direct electron ejection to the continuum and inner shell excitation followed by Auger transitions were included in the calculations. Multiple-ionization cross sections (for the production of an ion of any given ionization state from an ion of any given lower ionization state) were estimated utilizing measured values of electron loss probabilities for given inner shell vacancies in neutral krypton[11] and a simple model of Auger vacancy cascading in ions.[1] Although the techniques employed were highly approximate and the model used for atoms and ions relatively crude, reasonable estimates of the many cross sections required for the calculation of ionization rates were computed with relative economy of time and effort. Application of these results to a calculation of the cumulative ionization produced by an electron ring beam interacting with a krypton pressure "puff" indicated that Auger processes have a significant influence in speeding up ionization rates in such a system. Moreover, on the basis of the previous work by Hahn and Watson,[9] it is expected that the Auger contribution to ionization will be considerably enhanced for higher Z atoms and ions.

To study this effect in more detail, and in particular, to investigate the relative importance of Auger ionization over a range of target gas Z values, computations for neon, argon, and xenon similar to those previously made in Ref. 1 for krypton have been undertaken and the results are reported and discussed in this paper.

II. Calculational Procedures

The procedures used for computing the various ionization cross sections have been described in detail previously[1] and it suffices here to outline briefly the approach taken.

The energies of the impacting electrons in this work are considered to be in the relativistic range and large compared with the relevant electronic ionization potentials so that the Bethe-Born high energy approximation theory[6,7] is applicable. All target atoms or ions are considered to be in their ground state at the time of collision. Under these conditions the total cross section for ionization via direct transitions to the continuum for electrons of total energy E colliding with ions in ionization state Z_I is given by

$$\sigma^C(Z_I,E) = \sum_{n\ell} \sigma^C_{n\ell} \quad , \tag{1}$$

where the summation is taken over all subshells (n,ℓ), and

$$\sigma^C_{n\ell} = (\pi a_o^2) \frac{4\alpha_o^2}{\beta^2} \left[\ln \left(\frac{2\gamma\beta^2 E}{\Delta^C_{n\ell}} \right) - \beta^2 \right] g_{n\ell} \bar{M}^C_{n\ell} \, . \tag{2}$$

Here $a_o = 0.529 \times 10^{-8}$ cm is the Bohr radius, $\alpha_o = 1/137$ is the fine-structure constant, $\beta = v/c$ is the ratio of electron velocity to the velocity of light, $\gamma = (1 - \beta^2)^{-1/2}$, $\Delta^C_{n\ell}$ is an energy parameter of the order of the ionization potential of the (n,ℓ) subshell, $g_{n\ell}$ denotes the number of electrons in subshell (n,ℓ), and $\bar{M}^C_{n\ell}$ is the square of the electric-dipole-transition matrix element summed over the allowed continuum levels and averaged over the initial magnetic substates (electric-dipole parameter for continuum ionization).

Similarly, the total cross section for ionization due to excitation of inner shell electrons to unoccupied upper bound states followed by Auger transitions is given by

$$\sigma^A(Z_I,E) = \sum_{n\ell} \sigma^A_{n\ell} , \qquad (3)$$

such that

$$\sigma^A_{n\ell} = (\pi a_o^2) \frac{4\alpha_o^2}{\beta^2} \left[\ln \left(\frac{2\gamma\beta^2 E}{\Delta^B_{n\ell}} \right) - \beta^2 \right] g_{n\ell} \bar{M}^{Ex}_{n\ell} W_n , \qquad (4)$$

where $\Delta^B_{n\ell}$ is an energy parameter also of the order of the ionization potential of the (n,ℓ) sub-shell, $\bar{M}^{Ex}_{n\ell}$ is the corresponding electric-dipole parameter for excitation, and W_n is the Auger factor or normalized probability that a vacancy in the n^{th} shell will result in a readjustment process in which at least one Auger transition will occur between some pair of subshells.

The energy parameters $\Delta^C_{n\ell}$ and $\Delta^B_{n\ell}$ are approximated by

$$\Delta^C_{n\ell} = \Delta^B_{n\ell} = E_{n\ell} \qquad (5)$$

where $-E_{n\ell}$ are the IPM energy eigenvalues corresponding to subshell (n,ℓ) of the ion of ionization state Z_I. The procedures for evaluating the IPM eigenvalues and the dipole parameters $\bar{M}^C_{n\ell}$ and $\bar{M}^{Ex}_{n\ell}$ using the semi-classical projection operators developed by Hahn and Watson are described in detail in previous papers.[1,9]

Approximate values of the Auger factors W_n for neon, argon, and xenon ions were estimated from measured and theoretical x-ray and Auger transition probabilities and yields for neutral atoms.[12,13] Listed below are the non-zero values for W_n over the possible range of ionization states for each of the three species.

neon

$W_1 = 1.0$ $\quad 0 \leq Z_I \leq 6$

argon

$W_1 = 1.0$ $\quad 0 \leq Z_I \leq 6$

$W_1 = 0.84$ $\quad 7 \leq Z_I \leq 14$

$W_2 = 1.0$ $\quad 0 \leq Z_I \leq 6$

xenon

$W_1 = 0.9$ $\quad 0 \leq Z_I \leq 42$

$W_1 = 0.05$ $\quad 43 \leq Z_I \leq 50$

$W_2 = 0.9$ $\quad 0 \leq Z_I \leq 42$

$W_3 = 1.0$ $\quad 0 \leq Z_I \leq 24$

$W_4 = 1.0$ $\quad 0 \leq Z_I \leq 6$

The multi-ionization cross section for the creation of an ion of ionization state $Z_F = Z_I + j$ from an ion of ionization state Z_I in an electron-ion collision is given by

$$\sigma^{M}(Z_I,Z_F) = \sum_{n\ell} \sigma^{C}_{n\ell}(Z_I) S^{Z_I}_{n\ell}(j) + \sum_{n\ell} \sigma^{A}_{n\ell}(Z_I) X^{Z_I}_{n\ell}(j). \qquad (6)$$

Here $S^{Z_I}_{n\ell}(j)$ is the electron loss probability function which gives the probability that, in an electron-ion collision resulting initially in the ejection of an inner shell (n,ℓ) electron to the continuum, j electrons, including the initially ejected electron, will be emitted, and $X^{Z_I}_{n\ell}(j)$ is the corresponding electron-loss probability function for the process in which the inner shell electron is initially excited to an upper bound state. These functions are determined by the probabilities of Auger transitions, electron shake-off,[14] electron correlation effects[15] and other secondary processes which can lead to electron ejection following the creation of vacancies in various atomic subshells. In this treatment, we make the assumption that the rearrangement following the production of a vacancy due to excitation to an upper bound state will be the same as for continuum ionization and, therefore,

$$X^{Z_I}_{n\ell}(j) = S^{Z_I}_{n\ell}(j+1) \Big/ \sum_{k=2}^{L} S^{Z_I}_{n\ell}(k), \quad j > 0, \qquad (7)$$

where L is the upper limit on the number of electrons emitted following an ionizing collision.

The assumptions and procedures used in deriving the electron loss probability functions for neon, argon, and xenon ions are essentially those previously discussed in Ref. 1. For each of the three atomic species, the relative ion-abundance spectra arising from initial vacancies in the various sub-shells of the neutral as measured in the photo-ionization experiments of Carlson, et.al.,[11]

were used to obtain $S_{n\ell}^{Z_I}(j)$ for $Z_I = 0\text{-}3$. No ion abundance data were available for the valence shell of xenon and, as in the case of krypton, we have assumed that, for $Z_I = 0\text{-}3$, the production of a vacancy in the valence shell gives rise to 85% probability of one-electron emission and 15% probability of two-electron emission. For $Z_I > 3$, we have derived electron-loss probabilities by tracing, for an initial vacancy in each inner subshell, the dominant vacancy cascade path, taking into consideration the possibility of both Auger and radiative transitions with branching characterized by the values of Auger yields listed above. In the approximation used here, we have assumed that the dominant vacancy cascade path corresponds to an orderly stepwise propagation and multiplication of holes from shell to shell such that at each step where an Auger transition occurs, the Auger electron is ejected from the same shell as the electron which drops to the lower shell. (Actually, for initial vacancies in L or higher shells, the vacancy cascade is dominated by Auger transitions.) Examples of electron loss probabilities derived in this way for krypton ions were given in Ref. 1.

III. Computational Results and Discussion

A. Total Ionization Cross Sections

Total ionization cross sections for neon, argon, and xenon were computed using the method described above.

Plots of the cross sections for direct ionization to the continuum, σ^C; ionization due to inner shell excitation and subsequent Auger transitions, σ^A; and total ionization, σ^I; for neon, argon, krypton and xenon atoms and their ground state ions for an electron kinetic energy of 20 MeV are presented in Figs. 1-4. The krypton plot, reproduced from Ref. 1, is included in this series in order to provide a more complete picture of the systematic behavior of these cross sections with respect to atomic number of the target species. An examination of these curves strikingly demonstrates the fact, first pointed out by Hahn and Watson,[9] that although, for low Z species, direct continuum ejection is the important ionization mechanism, as Z becomes larger, the contribution of σ^A (associated with inner shell excitation) becomes more and more important, and, for high Z, dominates the total ionization cross section over much of the range of ionization states. (For all four neutrals, however, σ^C is considerably larger than σ^A.)

Thus for neon (Z = 10), σ^A is clearly of minor significance, whereas it becomes progressively more important with respect to σ^C for argon (Z = 18) and krypton (Z = 36). For xenon (Z = 54), it is apparent that σ^A dominates the total ionization process in the ranges Z_I = 2-6, Z_I = 11 - 24 and Z_I = 36 - 42. Thus, σ^A, at Z_I = 6 is more than 10 times larger, and at Z_I = 24, more than 12 times larger than the direct continuum cross section. As discussed previously in Ref. 1, the large

(orders of magnitude), discontinuous decreases in σ^A with increase in Z_I result from the elimination of Auger transitions originating from various shells following the depletion of electrons in those shells, whereas the small increases noted between the breaks occur because of the opening-up of new excitation channels as electrons are removed from previously filled subshells.

In Figs. 5-7, the continuum cross sections for neon, argon, and xenon are plotted again with respect to Z_I along with other estimates of these cross sections based on the extended treatment of Bethe-Born approximation theory for hydrogenic atoms and ions by Omidvar and Khateeb.[16,17] In these additional computations, the various ions are represented by a hydrogenic model. The results are quite similar to those observed for krypton.[1] For all three atoms, aside from the neutral (and the first ionization state in the case of neon), the hydrogenic estimates are always larger than the present results, reaching values for some ionization states which are up to three times higher than those obtained in the present study.

For the hydrogenic ions of the three atoms (Z_I = 9,17,53 for neon, argon, and xenon, respectively), however, for which the IPM potential becomes coulombic and where one might expect closer agreement, it is noted that a reasonable correspondence does exist between the cross section values obtained in the two sets of calculations. In each case, the value obtained in this study is about 33% smaller than the corresponding result of Omidvar and Khateeb, where the discrepancies arise from the approximations exployed in the present calculation as discussed previously.[1]

A check of the Hahn-Watson semi-classical projection operator technique can be made by comparing the computed values of the dipole excitation parameter, $\overline{M}_{10}^{Ex}$, for these various hydrogenic ions with the corresponding values obtained

from the data of Omidvar and Khateeb, which are given in their notation by $\sum_{n'} A(1,n')/4Z^2$ where the sum is taken over all $n' > 1$. The values obtained in the present calculation for neon, argon, and xenon ions are 7.53×10^{-3}, 2.32×10^{-3}, and 2.58×10^{-4}, respectively, as compared to the Omidvar and Khateeb values of 7.18×10^{-3}, 2.22×10^{-3}, and 2.46×10^{-4}, which constitutes agreement of better than 5%.

There appear to be essentially no experimental data with which we can compare these cross section results for the various rare gas ions. However, some recent experimental information is available on collisional ionization of neutral gases by high energy electrons. The total ionization cross sections obtained in the present investigation for electrons colliding with atomic neon, argon, and xenon respectively, over the energy range 0.01 - 20 MeV are plotted in Figs. 8 to 10 together with the curves obtained from the high energy studies of Rieke and Prepejchal[18] and the keV electron beam data of El-Sherbini, et.al.,[19] and Van der Wiel, et.al.[20] The experimental cross section points at 10, 12, and 14 keV were obtained from these last two references by summing the multiple-charge partial cross sections listed by the authors at each energy. For these three points, the collision energy is insufficient, in the case of xenon, for K-shell ionization. However, since K-shell ionization contributes a very small fraction to the total ionization, and since the dominant interactions leading to ionization occur in the outer shells with binding energies of at most a few hundred eV, it is assumed that the Bethe-Born theory has validity for estimating cross sections down to this limit.

For neon, agreement with the available experimental data lies within 15%, and for argon and xenon, within 35%, over the relevant range of electron energies.

B. Multi-Ionization in the Neutral Rare Gas Atoms

Van der Wiel, et.al.[20] and El Sherbini, et.al.[19] have, in a series of beam experiments, measured the cross sections for the formation of different charge states produced by the collision of electrons (multi-ionization cross sections) on various rare gas atoms for electron energies up to 14 keV. As a partial check on the methods used in our calculations, we have therefore computed multi-ionization cross sections for neutral neon, argon, and xenon at an electron energy of 14 keV, which, in accordance with our previous discussion, is considered to be within the realm of validity of the Bethe-Born formulation. The two sets of results at 14 keV are presented for comparison in Table I, where we have also included our previously computed values for krypton[1] in order to help reveal any Z-dependent systematic trends in the data. For xenon, good agreement exists between the two sets of values. For krypton and argon a fair correspondence is noted between all values except those for the higher charge states. For neon, however, considerable differences are observed between the cross section values except for those corresponding to single ionization. In general, the agreement improves markedly with increase in atomic number. However, two general trends of disagreement can be discerned.

The first is associated with the cross sections for the production of higher charge states. Thus for krypton, significant differences occur for ionization states 5 and 6 with the computed values decreasing much more rapidly with increase in ionization state than the electron beam cross sections. Similar behavior is also noted in the argon and neon data although in these cases, the large relative decline in the computed cross sections first becomes apparent for $Z_I = 4$. The observed higher charge states result basically from the creation of inner shell vacancies followed by reorganiza-

tional processes which lead to additional ionization. It is therefore difficult to isolate the specific causes of the observed deviations since they can arise either because of underestimates of the relevant inner shell cross sections or because of inadequacies in the electron-loss probabilities which were derived from photo-ionization measurements[11] rather than from data specific to electron collisional ionization.

The second area of disagreement concerns the magnitude of the cross-section for the production of the doubly charged ion relative to that of the singly charged particle. We note that for neon and argon, these ratios, obtained from the cross-sections computed in the present study are respectively 3.2 and 2.5 times the corresponding ratios obtained from the electron beam experiments. In this case, the deviations with respect to the electron-beam data can be attributed directly to the use of the outer-shell photo-ionization-derived electron loss probabilities on the following grounds.

Carlson[15] has shown that the relative abundances of doubly-charged ions that result from photo-ionization in the outer shells of neon and argon vary considerably with photon energy. In each case, the relative abundance increases significantly with increase in energy from the threshold (for double-ionization) until it finally levels off at an approximately constant ratio above about three times the threshold energy. The outer shell electron-loss-probabilities used in the present computations were based on these relatively high energy asymptotic ratios. Ionization by electron collision (at 14 keV) on the other hand, occurs predominantly with relatively low values of energy transfer.[21] In this range, according to the photo-ionization data, double (and higher multiple) ionization, which are attributed primarily to electron correlation effects, have a smaller probability of occurring. Thus the relative abundances of doubly charged ions observed in the electron-beam experiments can be expected to be smaller than those computed in this study.

C. Cumulative Ionization Produced by Relativistic Toroidal Electron Beams

We now apply these calculational procedures to the problem of computing the evolution in time of charged ion abundances resulting from the interaction of a relativistic toroidal electron beam with a pressure puff of an appropriate rare gas (ion loading in an electron ring device). In such a system, ions produced by these collisions are trapped in the potential well of the ring and successive impacts by the energetic electrons result in progression to higher and higher ionization states which, if charge transfer and electron recombination processes can be neglected, could lead, in principle to a fully stripped ion load. The problem has been treated previously for krypton using an idealized model for the electron ring and we refer to Ref. 1 for a discussion of the assumptions and equations used in this formulation. In the present study, we have assumed as representative parameters: ring volume $V = 1.2\ cm^3$, number of ring electrons $N_e = 10^{13}$, electron kinetic energy, $E_K = 20$ MeV, and gas profile parameters $T = \tau = 20\ \mu sec$ and $P_m = 5 \times 10^{-8}$ torr where the function representing the pressure is given by:

$$P(t) = \begin{cases} P_m t/T, & 0 \leqslant t \leqslant T \\ P_m \exp(-(t-T)/\tau), & t > T \end{cases} . \qquad (9)$$

Calculations by previous investigators[22,23] of ion stripping by an electron ring beam have been based on the assumption that the only relevant process is the stripping of one electron at a time by direct continuum ionization. We are primarily interested here in studying the

relative effect of Auger (and other atomic reorganizational processes) on ionization rates in such a system. We have therefore treated the problem in two ways for each atom considered. In the first, multi-ionization cross sections were estimated using Eq. (4) and the time dependences of the trapped ion abundances in the electron ring were computed. In the second, the time dependences were calculated considering only direct single-electron continuum ionization.

In Figs. 11 and 12, are shown, for xenon and argon, respectively, the time dependences of the ion abundances for several representative ion charge states, namely, Z_I = 1, 7, 17, 30, 44 and 54 (fully stripped ion) for xenon, and Z_I = 1, 4, 8, 13 and 18 (fully stripped ion) for argon. The solid curves correspond to the computations where only continuum ionization is considered, whereas the dashed curves represent the case where Auger processes are also computed. Clearly for xenon, Auger processes provide the dominant contribution to the ionization rates associated with the production in an electron ring of most of the charge states. Thus in Fig. 11, all of the charge state peaks shown except for Z_I = 1 and Z_I = 54, occur 3 to 5 times more rapidly in the case where Auger processes are taken into account than where continuum ionization alone is considered. The total time period associated with the formation of the fully-stripped ions, however, is determined mainly by the very long intervals required to strip off the last few electrons (due to the very small cross sections with negligible Auger contributions for highly ionized atoms) and on a relative basis therefore, differ only slightly for the two calculations. For argon, also, as noted in Fig. 12, Auger processes make a significant contribution to ion production rates, although for this lower Z species, the effect is much less pronounced. In this case, there is at most a factor of two speed-up in the production of individual charge states.

Similar computations have been made for neon (lowest in atomic number of all the gases studied), but the Auger contributions for this species were found to be relatively insignificant. On the other hand, krypton (see Fig. 4 in Ref. 1), lying in atomic number between argon and xenon shows an Auger speed-up intermediate to that of argon and xenon, amounting to as much as a factor of 3 for some charge states. These results clearly demonstrate the progressively increasing importance, with increasing atomic number, of these inner-shell processes on charge state production in such devices, and indicate that for target atoms with Z greater than about 50, Auger ionization processes dominate at most stages of ionization.

Acknowledgments

The author would like to thank Dr. J.M. Peterson for first calling attention to the potential importance of Auger processes in electron ring ionization, Dr. Y. Hahn for a number of very informative discussions and Drs. L.J. Laslett, D. Keefe, G.R. Lambertson, R.W. Schmieder, W.W. Chupp, and J.B. Rechen for helpful comments in relation to this work.

References

1. A. Salop, Phys. Rev. A, 8, 3032 (1973).
2. V.I. Veksler, et.al. in Proceedings of the VI International Conf. on High Energy Accelerators, Cambridge Electron Accelerator CEAL-2000, 1967 (unpublished), p. 289.
3. D. Keefe, Part. Accel. 1, 1 (1970).
4. J.E. Eninger, Nucl. Instrum. Methods 97, 19 (1971).
5. See collected papers in IEEE Trans. Nucl. Sci. NS-19, 22 (1972).
6. H. Bethe, Ann. Phys. 5, 325 (1930).
7. N.F. Mott and H.S.W. Massey, The Theory of Atomic Collisions (Oxford U.P., Oxford England, 1965), Chap. 16.
8. Y. Hahn and K.M. Watson, Phys. Rev. A 6, 548 (1972).
9. Y. Hahn and K.M. Watson, Phys. Rev. A 7, 491 (1973).
10. A.E.S. Green, D.L. Sellin, and A.S. Zachor, Phys. Rev. 184, 1 (1969).
11. T.A. Carlson, W.E. Hunt, and M.O. Krause, Phys. Rev. 151, 41 (1966).
12. E.H.S. Burhop and W.S. Asaad, in Advances in Atomic and Molecular Physics VIII, edited by D.R. Bates and I. Esterman (Academic, New York, 1972), p. 163.
13. W. Bambynek, B. Crasemann, R.W. Fink, H.U. Freund, H. Mark, C.D. Swift, R.E. Price, and P.V. Rao, Rev. Mod. Phys. 44, 716 (1972).
14. T.A. Carlson, C.W. Nestor, Jr., T.C. Tucker and F.B. Malik, Phys. Rev. 169, 27 (1968).
15. T.A. Carlson, Phys. Rev. 156, 142 (1967).
16. K. Omidvar and A.H. Khateeb, J. Phys. B 6, 341 (1973).
17. K. Omidvar (private communication).
18. F.F. Rieke and W. Prepejchal, Phys. Rev. A 6, 1507, (1972).
19. Th. M. El-Sherbini, M.J. van der Wiel, and F.J. de Heer, Physica 48, 157 (1970).
20. M.J. van der Wiel, Th. M. El-Sherbini and L. Vriens, Physica 42, 411 (1969).

21. E.W. McDaniel, Collision Phenomena in Ionized Gases (John Wiley & Sons, Inc.) New York, 1964) p.211.

22. L.J. Laslett and B.S. Levine, Lawrence Berkeley Laboratory Internal Report No. ERAN-202, 1972 (unpublished).

23. G.S. Janes, Lawrence Berkeley Laboratory Internal Report No. ERAN-17, (1968) (unpublished).

Figure Captions

1. The estimated ionization cross-sections, σ^C, σ^A, and σ^I for 20 MeV electrons on neutral neon and all of its ground state ions. In this and the following three figures, σ_c is the cross section for direct ejection to the continuum, σ^A, the cross-section corresponding to excitation to unoccupied bound states followed by Auger emission, and σ^I, the sum of σ^C and σ^A. The "curves" for this and the following six figures were obtained by drawing straight line segments between the cross-section points computed for each ionization state.

2. The estimated ionization cross-sections, σ^C, σ^A and σ^I for 20 MeV electrons on neutral argon and all of its ground state ions.

3. The estimated ionization cross-sections, σ^C, σ^A, and σ^I for 20 MeV electrons on neutral krypton and all of its ground state ions.

4. The estimated ionization cross-sections, σ^C, σ^A and σ^I for 20 MeV electrons on neutral xenon and all of its ground state ions.

5. Comparison of direct continuum ionization cross-sections computed for 20 MeV electrons on neon and its ions with other estimates based on a hydrogenic model using the formulation of Omidvar and Khateeb (Refs. 16 and 17).

6. Comparisons of direct continuum cross-sections computed for 20 MeV electrons on argon and its ions with other estimates based on a hydrogenic model using the formulation of Omidvar and Khateeb (Refs. 16 and 17).

7. Comparison of direct continuum cross-sections computed for 20 MeV electrons on xenon and its ions with other estimates based on a hydrogenic model using the formulation of Omidvar and Khateeb (Refs. 16 and 17).

8. Comparison of the estimated total ionization cross-sections for electrons on neon atoms with available experimental data over the energy range from 0.01 to 20 MeV. The experimental curve is a plot of the Bethe asymptotic formula with the parameters for neon listed by

Rieke and Prepejchal. (See Ref. 18). The experimental points are obtained from Ref. 20.

9. Comparison of the estimated total ionization cross-sections for electrons on argon atoms with available experimental data over the energy range from 0.01 to 20 MeV. The experimental curve is a plot of the Bethe asymptotic formula with the parameters for argon listed by Rieke and Prepejchal (See Ref. 19). The experimental points are obtained from Ref. 20.

10. Comparison of the estimated total ionization cross-sections for electrons on xenon atoms with available experimental data over the energy range from 0.01 to 20 MeV. The experimental curve is a plot of the Bethe asymptotic formula with the parameters for Xenon listed by Rieke and Prepejchal. (See Ref. 19). The experimental points are obtained from Ref. 19.

11. Time dependences of the trapped ion abundances for several representative xenon ionization states resulting from the interaction of a 20 MeV electron ring beam with a xenon gas "puff". Each abundance profile is designated by the degree of ionization. The results obtained assuming only direct continuum ionization are presented as the solid curves whereas those derived by also including the effects of Auger processes are shown as the dashed curves. Also shown is the time dependence of the neutral xenon abundance within the ring volume. The ring has a mean radius of 3 cm. and contains 10^{13} electrons within an assumed fixed volume of 1.2 cm^3.

12. Time dependences of the trapped ion abundances for several representative argon ionization states resulting from the interaction of a 20 MeV electron ring beam with an argon gas "puff". The description is the same as that given in Fig. 11.

Table I - Multi-ionization Collision Cross-sections for 14 keV Electrons on Neutral Rare Gas Atoms.

Atom	Final Ionization State	Cross Section (10^{-18} cm^2) Experimental[a]	Present
Xenon	1	8.5	7.5
	2	2.9	3.0
	3	1.86	1.35
	4	0.86	0.86
	5	0.26	0.26
	6	0.15	0.08
Krypton	1	9.0	8.2
	2	1.41	2.5
	3	0.99	0.87
	4	0.26	0.16
	5	0.089	0.028
	6	0.041	0.007
Argon	1	8.11	5.6
	2	0.65	1.12
	3	0.214	0.162
	4	0.046	0.015
	5	0.007	0.001
Neon	1	3.67	3.60
	2	0.163	0.509
	3	0.015	0.036
	4	0.002	0.0005

[a] Experimental cross sections were obtained from Ref. 19 for xenon and krypton and from Ref. 20 for argon and neon.

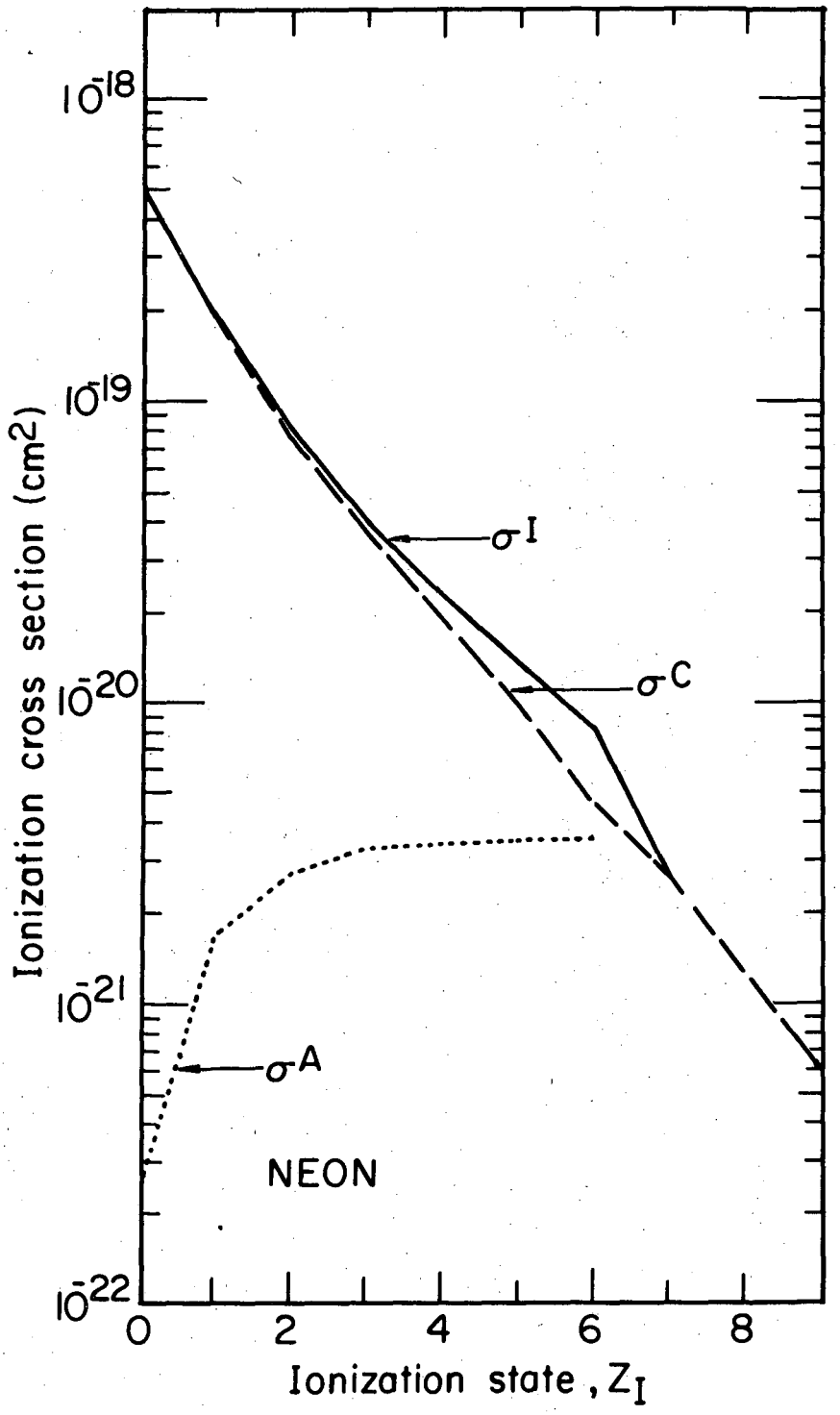
10^{-18}
10^{-19}
10^{-20}
10^{-21}
10^{-22}
Ionization cross section (cm^2)
σI
σC
σA
NEON
0
2
4
6
8
Ionization state, Z_I
XBL7311-4478

Figure 1

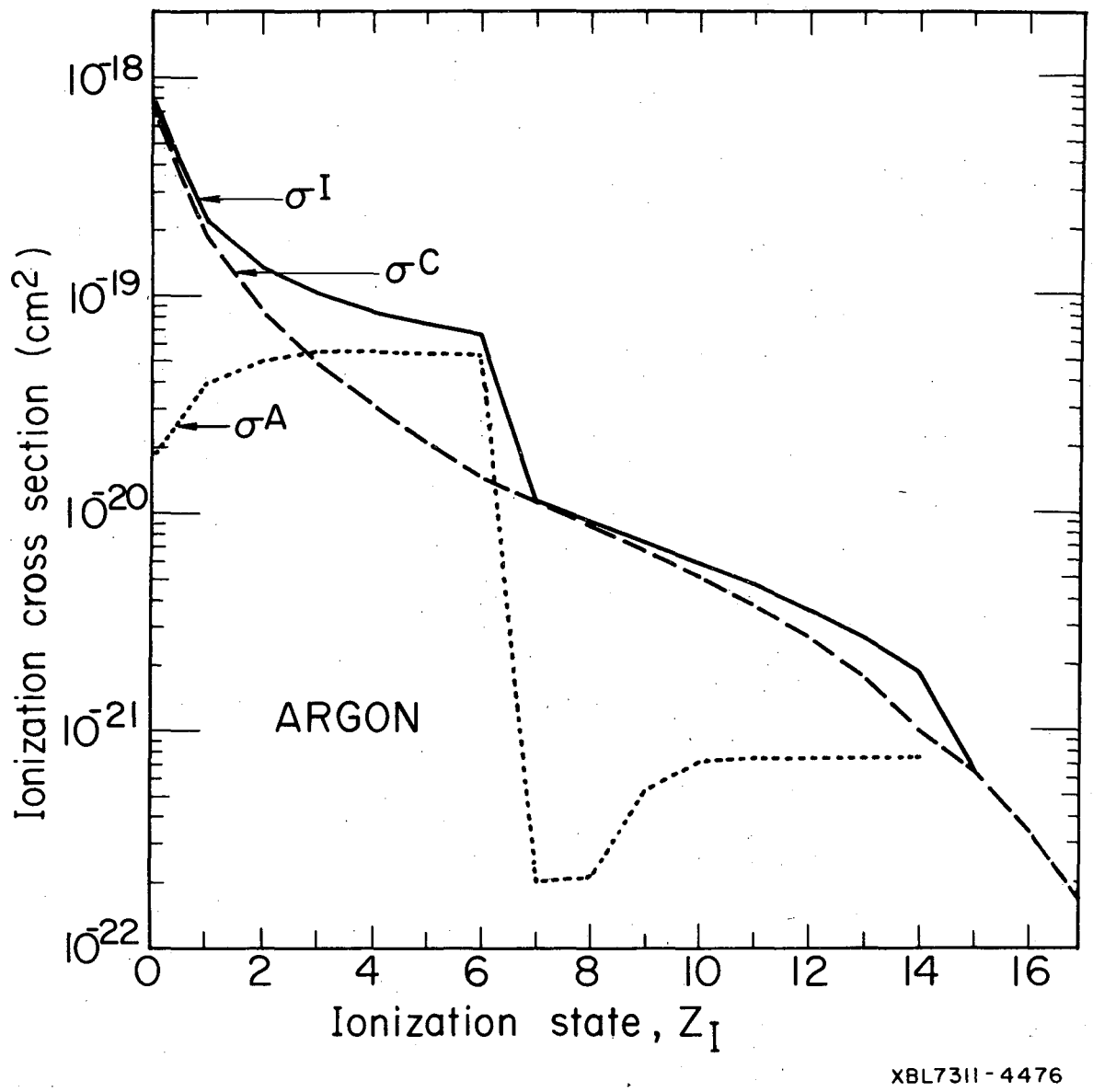
10^{-18}
10^{-19}
10^{-20}
10^{-21}
10^{-22}
Ionization cross section (cm^2)
σI
σC
σA
ARGON
0
2
4
6
8
10
12
14
16
Ionization state, Z_I
XBL7311-4476

Figure 2

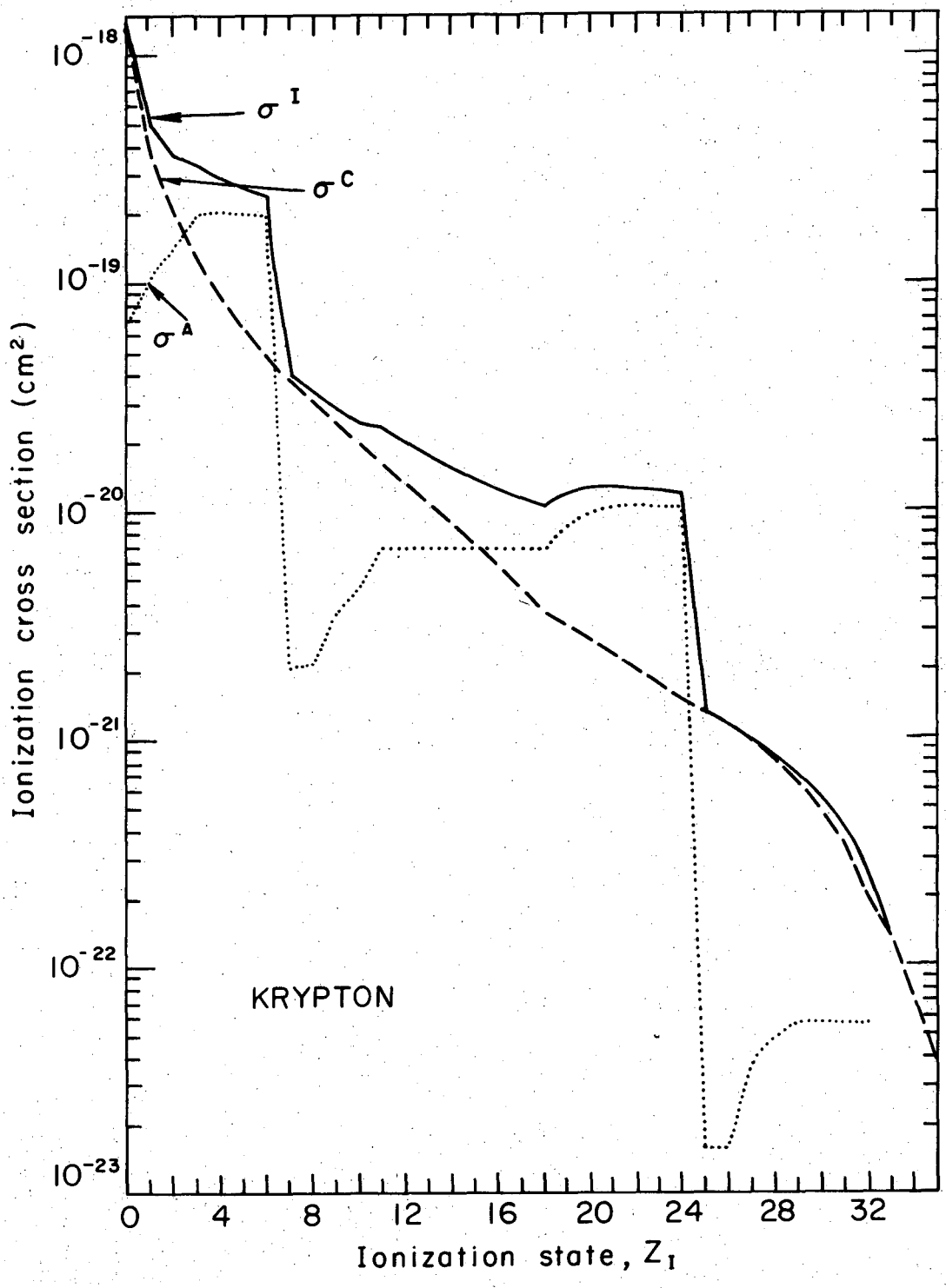

XBL736-3046

Figure 3

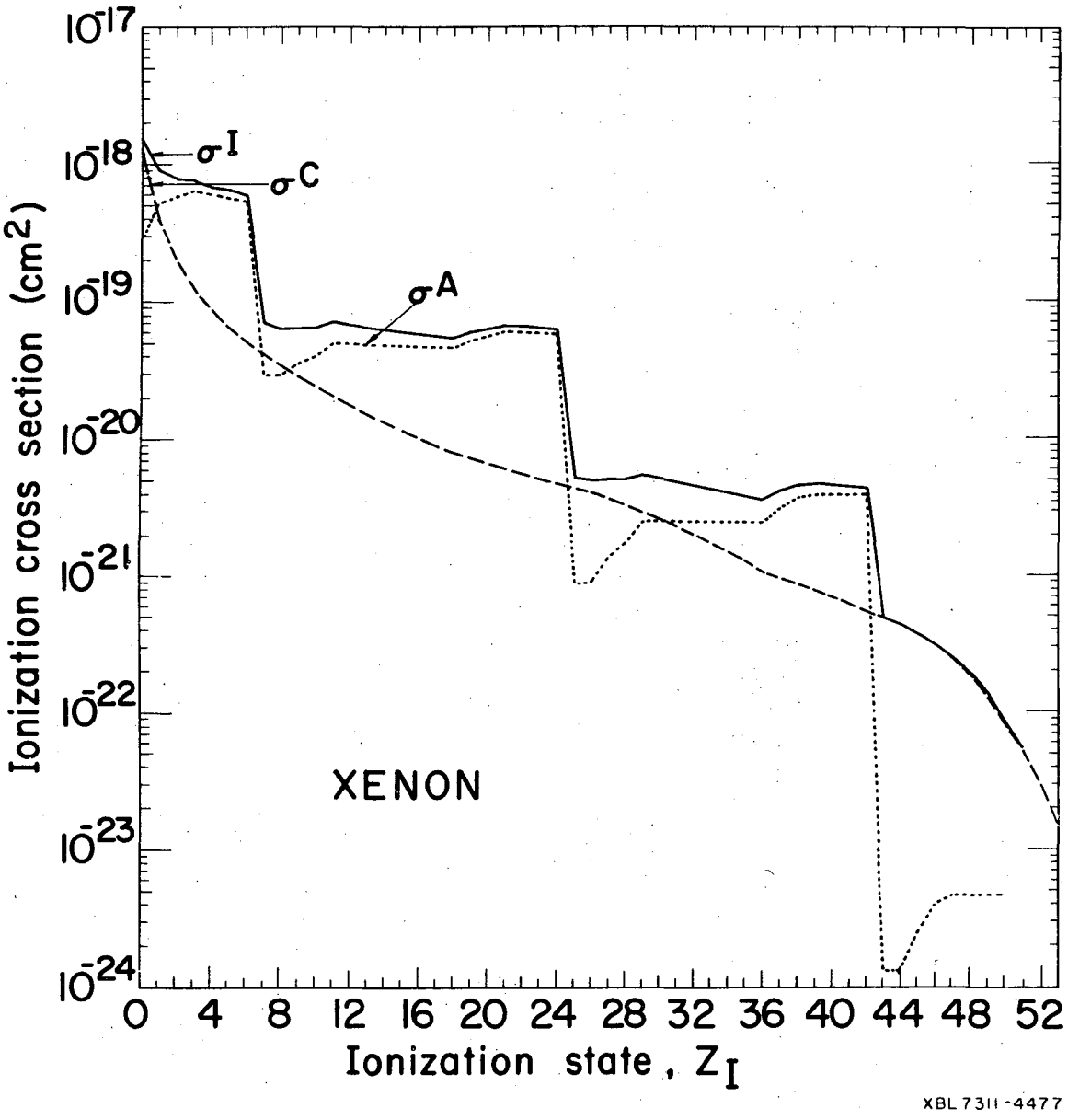
Ionization cross section (cm2)
10-17
10-18
10-19
10-20
10-21
10-22
10-23
10-24
σI
σC
σA
XENON
0 4 8 12 16 20 24 28 32 36 40 44 48 52
Ionization state, ZI
XBL 7311-4477

Figure 4

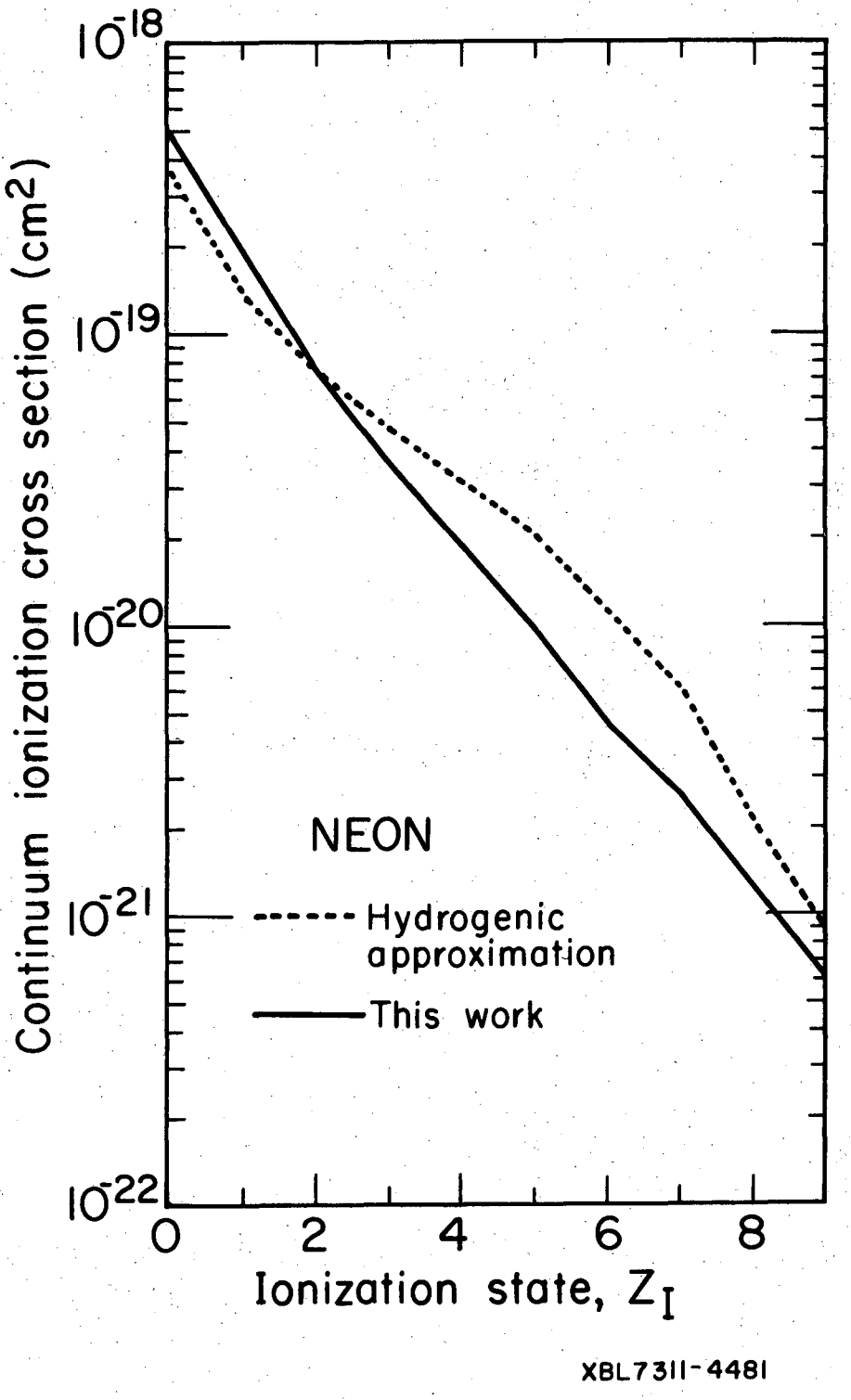
Continuum ionization cross section (cm²)
10⁻¹⁸
10⁻¹⁹
10⁻²⁰
10⁻²¹
10⁻²²
NEON
Hydrogenic approximation
This work
0
2
4
6
8
Ionization state, Z_I
XBL7311-4481

Figure 5

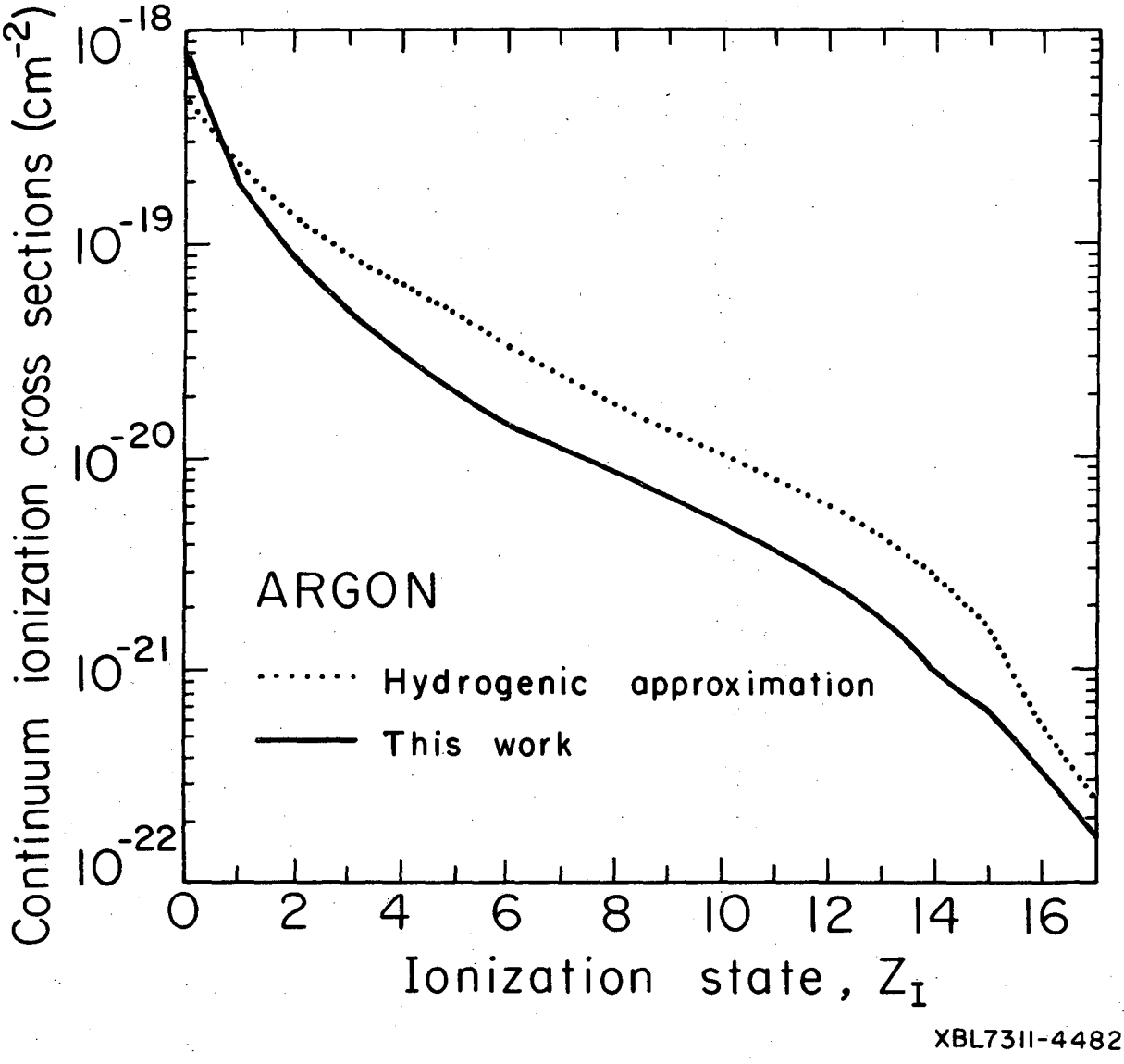
Continuum ionization cross sections (cm^{-2})
10^{-18}
10^{-19}
10^{-20}
10^{-21}
10^{-22}
ARGON
Hydrogenic approximation
This work
0
2
4
6
8
10
12
14
16
Ionization state, Z_I
XBL7311-4482

Figure 6

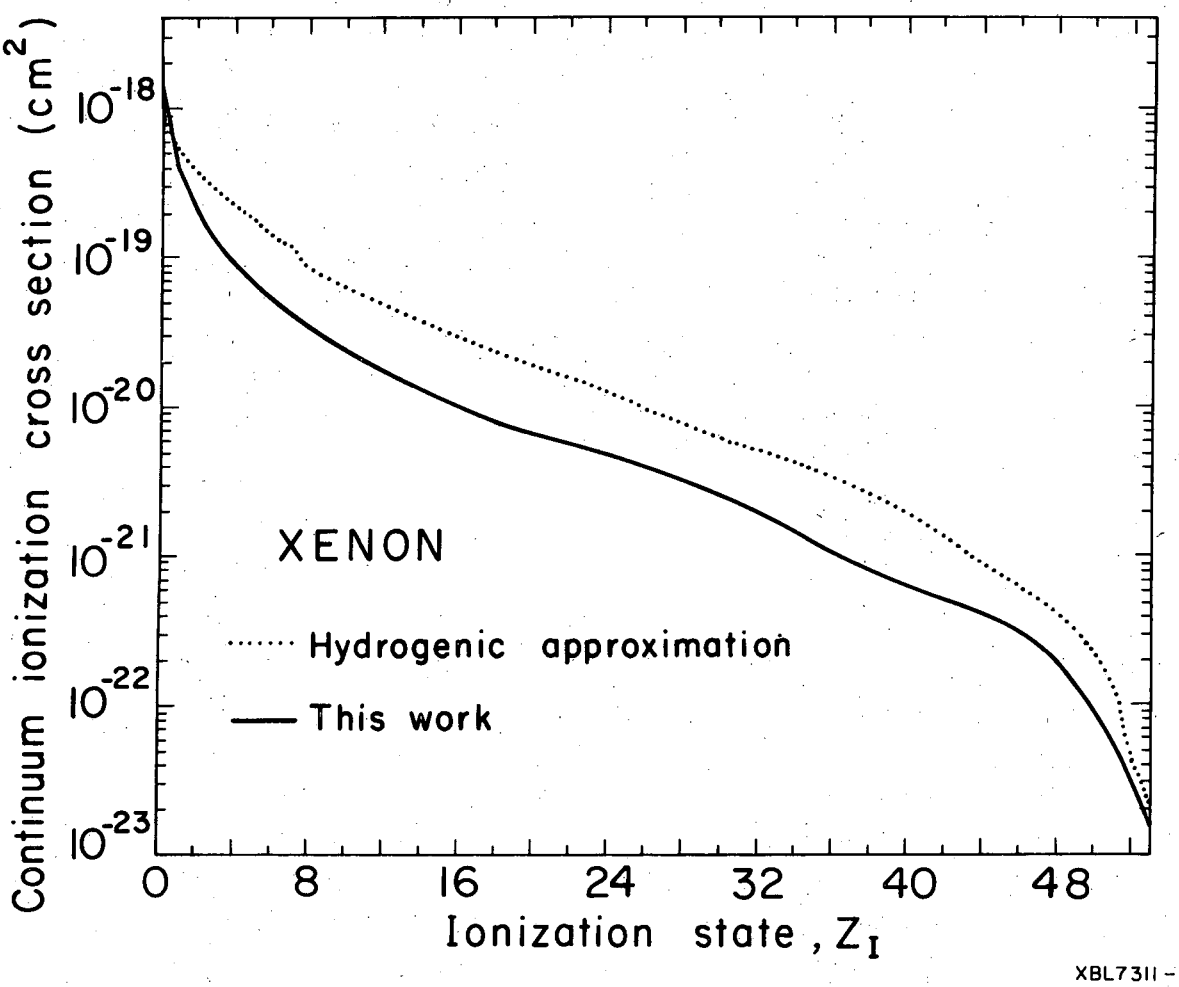
Continuum ionization cross section (cm^2)
10^{-18}
10^{-19}
10^{-20}
10^{-21}
10^{-22}
10^{-23}
XENON
Hydrogenic approximation
This work
0
8
16
24
32
40
48
Ionization state, Z_I
XBL7311 - 4483

Figure 7

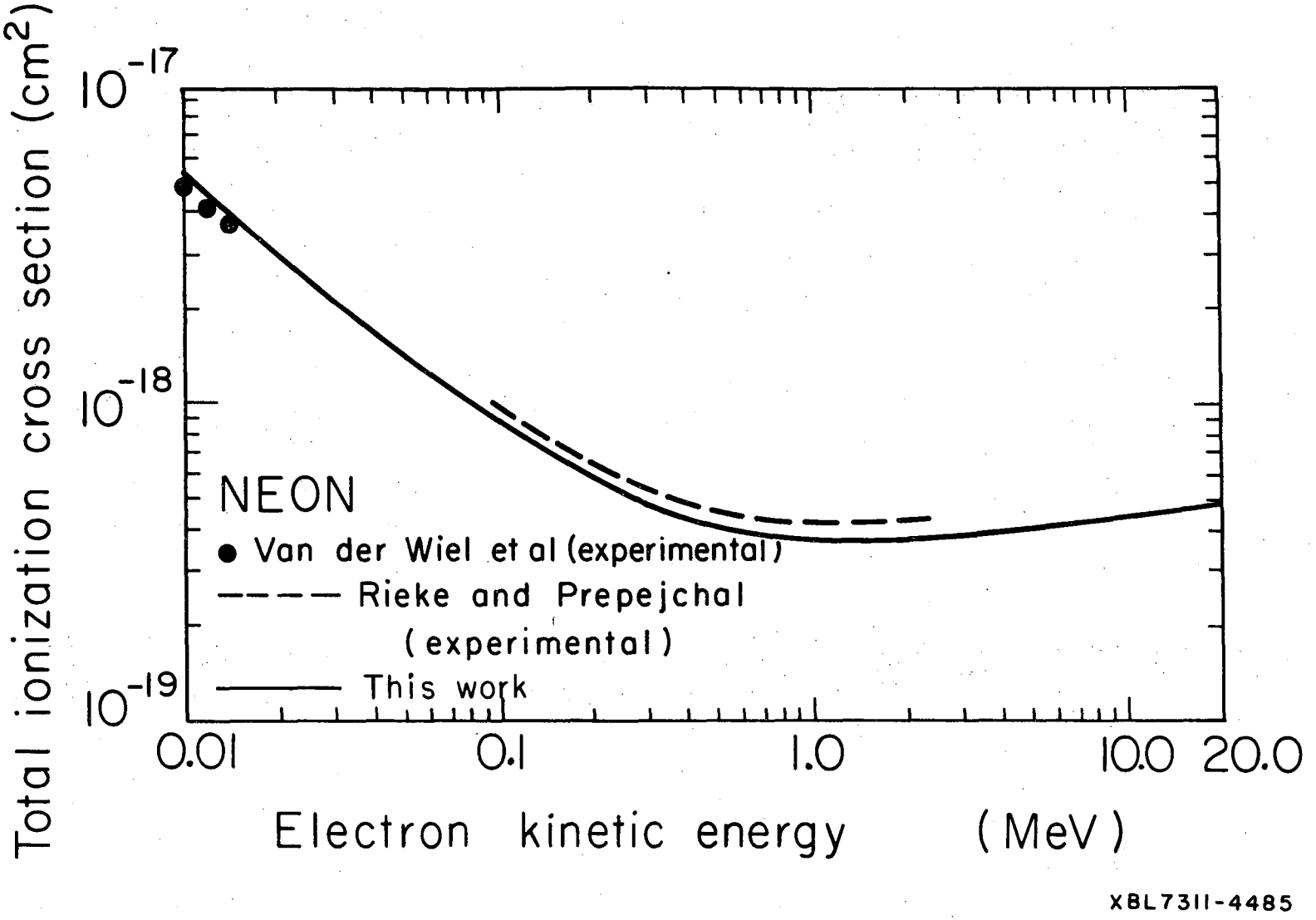
Total ionization cross section (cm²)
10⁻¹⁷
10⁻¹⁸
10⁻¹⁹
NEON
● Van der Wiel et al (experimental)
– – – – Rieke and Prepejchal (experimental)
——— This work
0.01
0.1
1.0
10.0
20.0
Electron kinetic energy (MeV)
XBL7311-4485

Figure 8

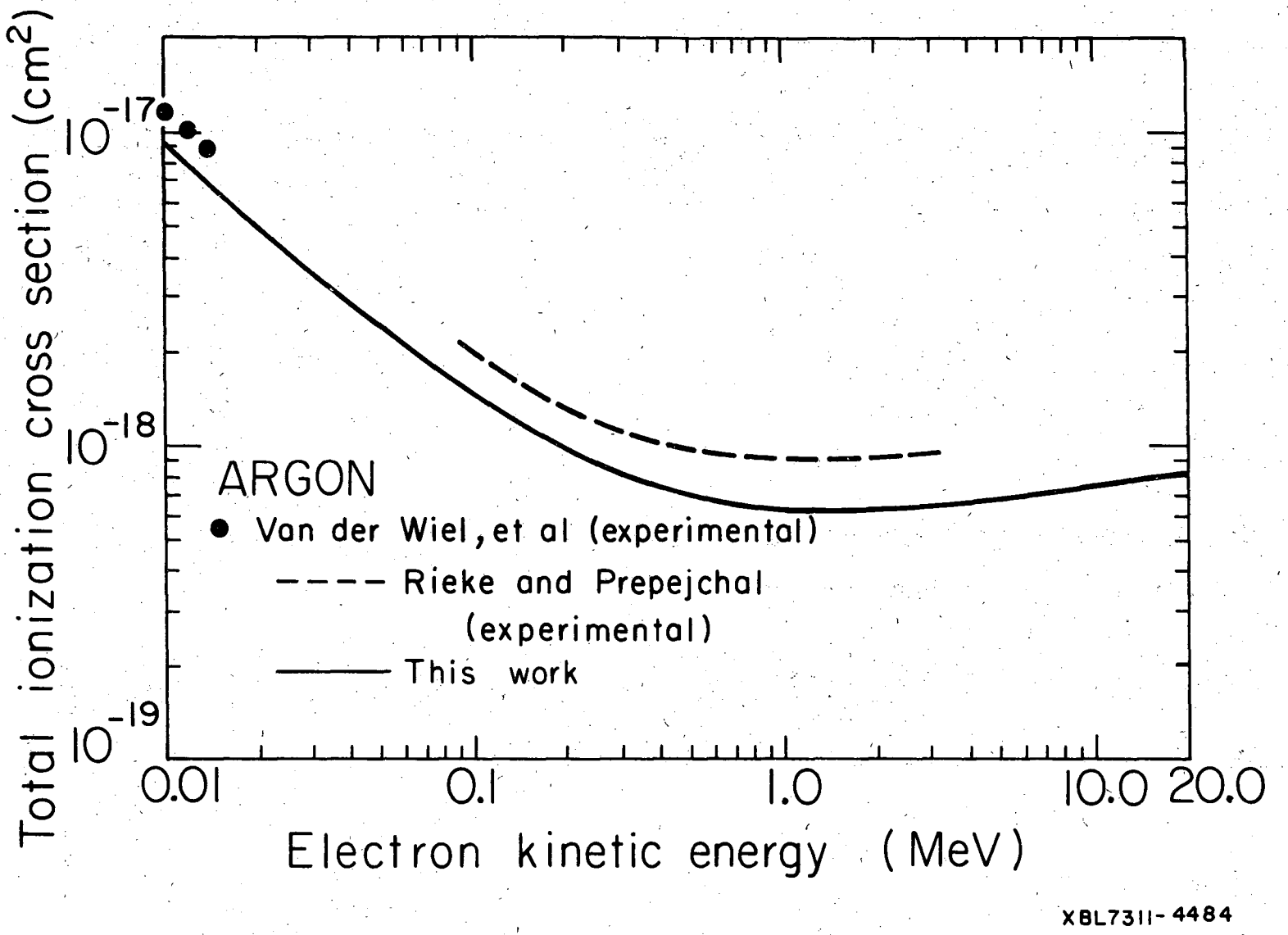
Total ionization cross section (cm²)
10⁻¹⁷
10⁻¹⁸
10⁻¹⁹
ARGON
Van der Wiel, et al (experimental)
Rieke and Prepejchal (experimental)
This work
0.01
0.1
1.0
10.0
20.0
Electron kinetic energy (MeV)
XBL7311-4484

Figure 9

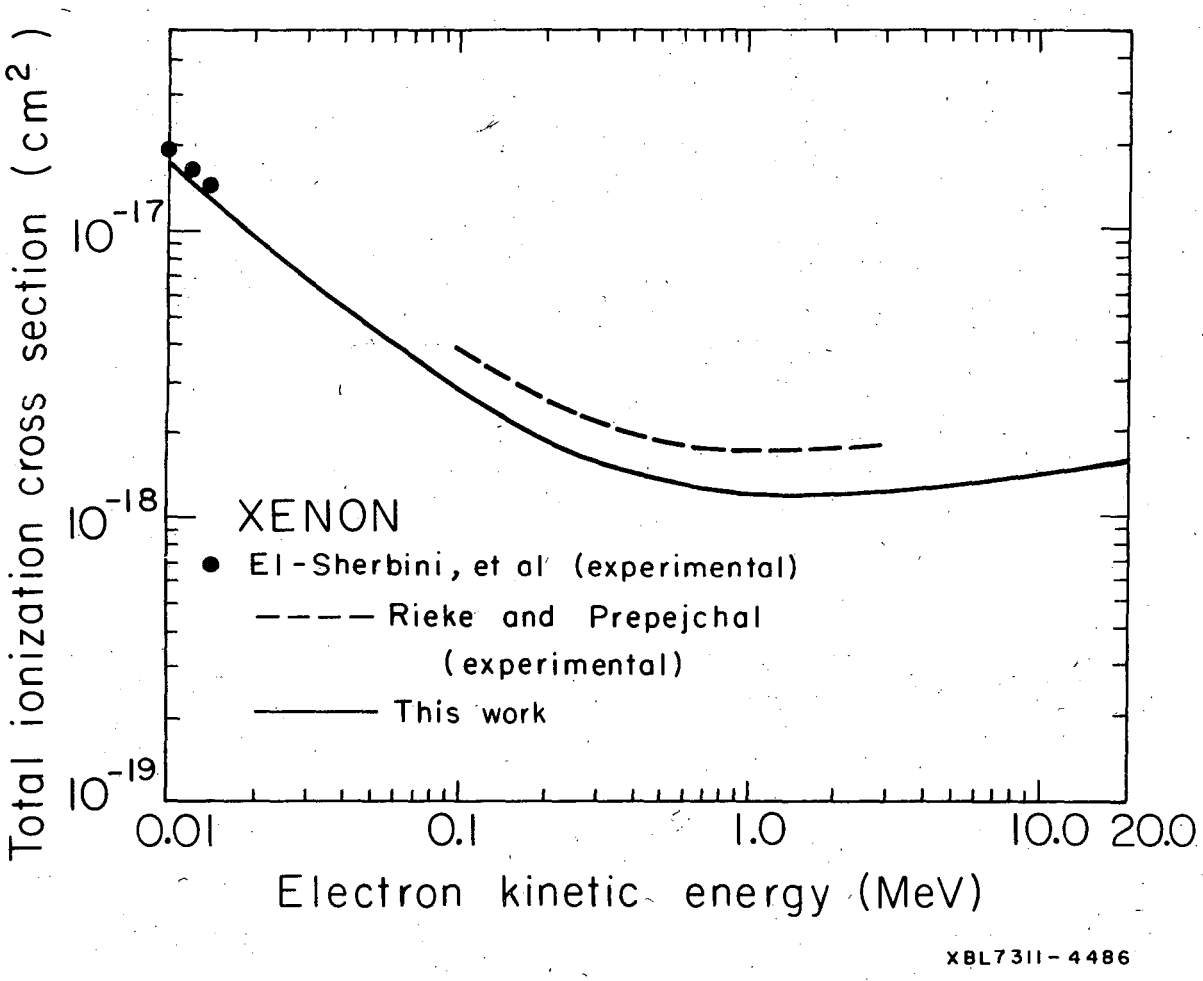
Total ionization cross section (cm²)
10⁻¹⁷
10⁻¹⁸
10⁻¹⁹
XENON
El-Sherbini, et al (experimental)
Rieke and Prepejchal (experimental)
This work
0.01
0.1
1.0
10.0
20.0
Electron kinetic energy (MeV)
XBL7311-4486

Figure 10

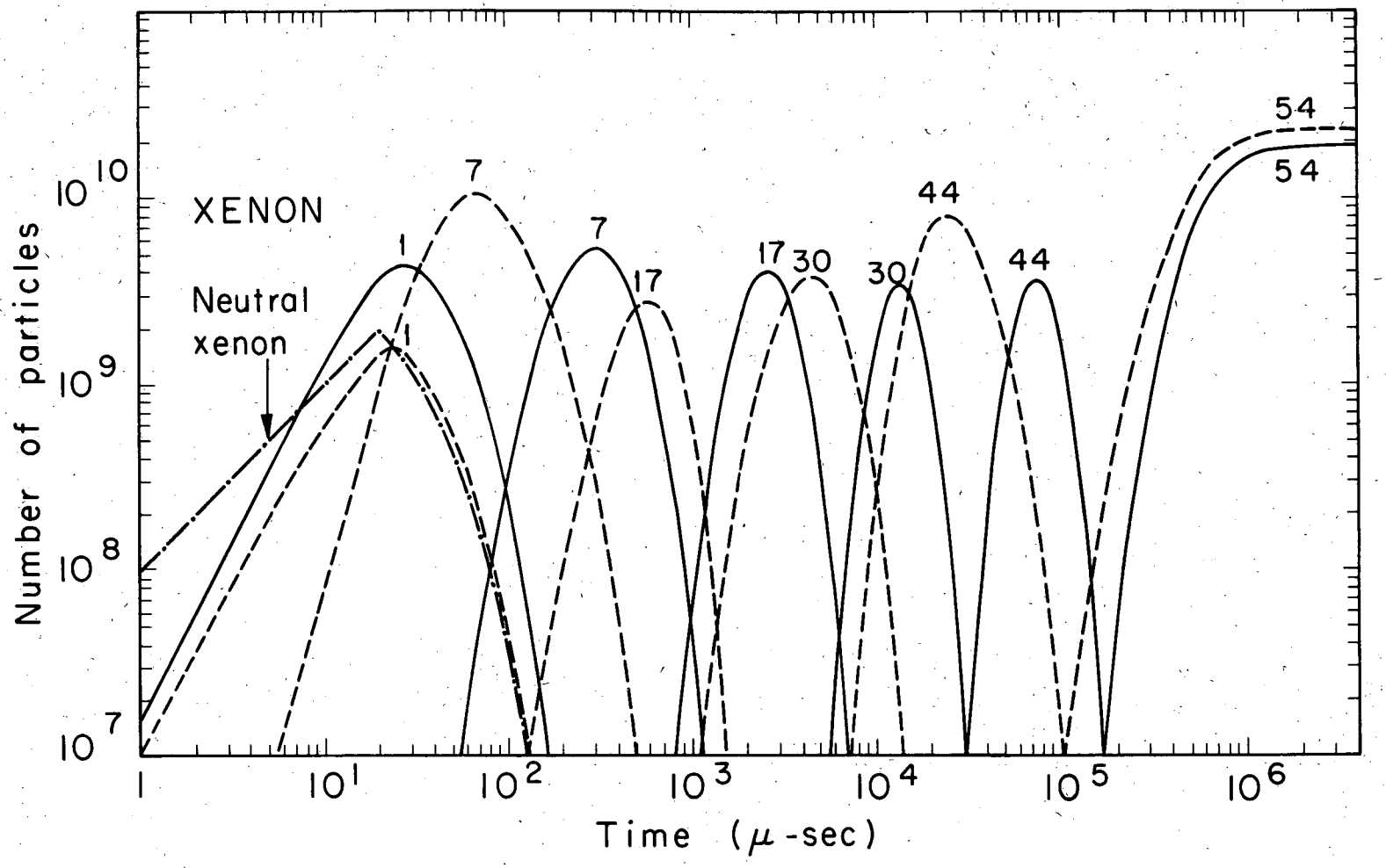
XENON
Neutral xenon
Number of particles
Time (μ-sec)
1
7
17
30
44
54
XBL 7311-4480

Figure 11

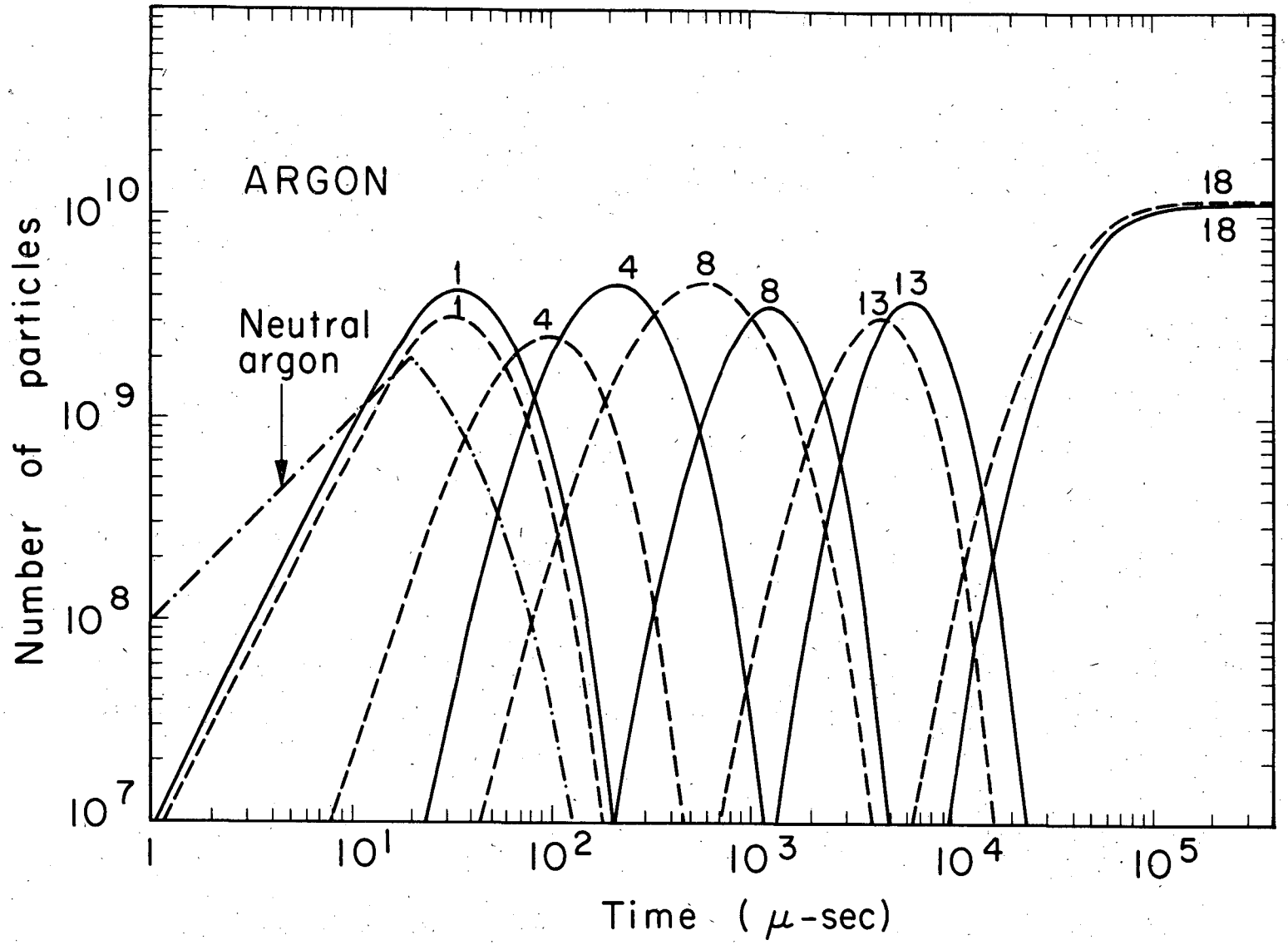
ARGON
Neutral argon
Number of particles
Time (μ-sec)
1
4
8
13
18
XBL7311 - 4479

Figure 12

TECHNICAL INFORMATION DIVISION
LAWRENCE BERKELEY LABORATORY
UNIVERSITY OF CALIFORNIA
BERKELEY, CALIFORNIA 94720